PROCEEDINGS A

rspa.royalsocietypublishing.org

Research

Cite this article: Huynen A, Detournay E, Denoël V. 2016 Eulerian formulation of elastic rods. *Proc. R. Soc. A* **472**: 20150547. http://dx.doi.org/10.1098/rspa.2015.0547

Received: 6 August 2015
Accepted: 31 May 2016

Subject Areas:
mechanics

Keywords:
elastic rod, Eulerian formulation, self-feeding

Author for correspondence:
Alexandre Huynen
e-mail: alexandre.huynen@gmail.com

Electronic supplementary material is available at http://dx.doi.org/10.1098/rspa.2015.0547 or via http://rspa.royalsocietypublishing.org.

THE ROYAL SOCIETY PUBLISHING

Eulerian formulation of elastic rods

Alexandre Huynen[1,2,3], Emmanuel Detournay[2] and Vincent Denoël[1]

[1]Division of Structural Engineering, Department of Architecture, Geology, Environment and Constructions, University of Liège, Liège, Belgium
[2]Department of Civil, Environmental and Geo-Engineering, University of Minnesota, Minneapolis, MN, USA
[3]F.R.I.A., F.R.S.–FNRS, National Fund for Scientific Research, Brussels, Belgium

AH, 0000-0001-9771-6926

In numerous biological, medical and engineering applications, elastic rods are constrained to deform inside or around tube-like surfaces. To solve efficiently this class of problems, the equations governing the deflection of elastic rods are reformulated within the Eulerian framework of this generic tubular constraint defined as a perfectly stiff normal ringed surface. This reformulation hinges on describing the rod-deformed configuration by means of its relative position with respect to a reference curve, defined as the axis or spine curve of the constraint, and on restating the rod local equilibrium in terms of the curvilinear coordinate parametrizing this curve. Associated with a segmentation strategy, which partitions the global problem into a sequence of rod segments either in continuous contact with the constraint or free of contact (except for their extremities), this re-parametrization not only trivializes the detection of new contacts but also transforms these free boundary problems into classic two-points boundary-value problems and suppresses the isoperimetric constraints resulting from the imposition of the rod position at the extremities of each rod segments.

1. Introduction

A wide scope of disciplines ranging from medical science to engineering is concerned with the constrained deformation of a slender elastic body. With the nature of the constraint being contingent on the context,

the elastic body, which is generally referred to as a *rod*, may be coiled/wound around another slender body or restrained inside a straight or sinuous conduit.

Applications of this general problem include the insertion of miniature instruments into blood vessels for the treatment of vascular and cerebrovascular pathologies (e.g. abdominal and thoracic aortic aneurysms, stroke) as well as the endoscopic examination of internal organs (see for instance [1,2]). Another application concerns the petroleum industry, which relies on kilometres-long drillstrings to transmit the axial force and torque necessary to drill the rock formations and reach deep hydrocarbon reservoirs [3,4]. At very small lengthscales, the wrapping of DNA around histone cores [5–8] or carbon nanotubes [9] has recently been the subject of intensive research in biophysics. Finally, twining plants, which achieve vertical growth through the friction generated by revolving around poles or other supports [10,11], constitute a further natural manifestation of this relatively broad class of problems.

As discrete and/or continuous contacts develop between the rod and the constraint, modelling of these phenomena usually implies the partitioning of the global problem into a set of boundary-value problems [12,13] specifying both the position and inclination of the rod at its extremities. Each elementary problem corresponds to a segment of rod either in continuous contact with the constraint or free of contact (between its extremities.) The length of the rod spanning each elementary problem and satisfying the associated boundary conditions is, however, *a priori* unknown and, therefore, constitutes an inherent part of the solution. This feature, specific to (one-dimensional) free boundary problems [14], is also encountered in other applications, e.g. the continuous casting process and the extrusion of plastic through a draw plate [15], the laying of subsea cables and pipelines [16,17] or, in slightly different configurations, the elastically deformable arm scale [18] and the self-encapsulation of elastic rods [19]. Resorting to a conventional Lagrangian approach, the axially unconstrained nature of these problems, referred to as *self-feeding* in the following, combined with the boundary conditions specifying the rod location at both extremities lead to the establishment of integral constraints (namely isoperimetric constraints) on the unknown length of the rod.

The rod is further compelled to satisfy a non-penetration requirement ensuring that, depending on the context, the rod remains either inside or outside the constraint. The assessment of this unilateral contact condition requires, in principle, the comparison of two curves parametrized by distinct curvilinear coordinates (i.e. the rod and the constraint axis), an intensive computational task contributing to the numerical burden associated with conventional approaches.

For planar elastica, the above-mentioned difficulties have been circumvented by adopting a Eulerian description of the rod in terms of the curvilinear coordinate associated with the constraint [20,21] and by describing its deformed configuration by means of the signed distance between the rod and the axis of the constraint [22]. This approach has been shown to drastically simplify the resolution of the constrained problem by trivializing the assessment of the unilateral contact condition and limiting the degeneracy of the governing equations with diminishing clearance or bending stiffness. Generalizing these concepts, this paper aims to extend this formulation to three-dimensional configurations. In the following, the special Cosserat rod theory is reformulated within the Eulerian framework of a generic constraint defined as a perfectly stiff normal ringed surface. The axis or spine curve associated therewith, referred to as *reference curve* independently of the constraint nature, is further assumed to be known and regular (i.e. its tangent vector being everywhere well defined.) The proposed Eulerian reformulation hinges on describing the rod-deformed configuration by means of its relative position with respect to the reference curve and expressing the kinematical as well as mechanical quantities pertaining to the rod in terms of the curvilinear coordinate associated with the reference curve, rather than the rod. As the *a priori* unknown domain, *viz.* the rod length, is substituted for the known reference curve, the free boundary problem and the associated isoperimetric constraints are converted into a classical two-point boundary-value problem for which the rod eccentricity with respect to the reference curve is prescribed at both extremities of the domain.

(a) Nomenclature

Lower case letters (Latin and Greek) are used to denote kinematic quantities pertaining to the rod while upper case is preferred for variables describing the reference curve and the constraint surface. For instance, we denote by s the Lagrangian coordinate, identifying a rod cross section along its centreline, and by S the Eulerian coordinate, identifying a section along the reference curve. Additionally, vectors of the Euclidean space $\mathbb{E}^3$ are denoted by boldface italic symbols such as $\boldsymbol{u}$, and calligraphic symbols (bold and plain) are used to denote dimensionless quantities, e.g. $\mathcal{F}_j$. Einstein summation convention is implied and, unless otherwise stated, subscripts i and j have range over 1,2 and 1,2,3, respectively.

2. Lagrangian formulation

(a) Problem definition

Let us define the right-handed orthonormal basis $\{\boldsymbol{e}_j\}$ for the Euclidean space $\mathbb{E}^3$ and denote by $\boldsymbol{R}(S) = X_j\boldsymbol{e}_j$, the parametrization of the reference curve $\mathscr{C}$. The parameter S, referred to as the *Eulerian coordinate*, identifies a section along $\mathscr{C}$ which consists of all points whose reference position is on the plane perpendicular to the reference curve at S. Without loss of generality, the parametrization of the reference curve is assumed to be natural or arc-length, so that its tangent is a unit vector. The constraint surface, considered frictionless and undeformable, is the normal ringed surface [23] generated by sweeping a circle of radius $Q(S)$ centred on the reference curve and in the normal plane to $\mathscr{C}$.

The elementary problem considered in this paper consists of a segment of rod, either in continuous contact with the constraint or free of contact between its extremities, that is forced to go through two fixed points in space while being subjected to both a distributed body force and a body couple. As already noted, the unknown length of the rod is free to adjust to both the external loading and the boundary conditions acting at the rod extremities. Prescribing the rod position and inclination at these points, this self-feeding feature may be obtained by imposing one extremity of the rod to be clamped while considering the other to be moving freely through a frictionless sliding sleeve. The rod, initially straight, is assumed to behave as a one-dimensional elastic body according to the special Cosserat theory of rods. Although readily extendable to encompass effects of shear and extensibility, the present reformulation is, for the sake of brevity, restricted to rods that can undergo large deformations in space by experiencing bending and torsion.

The continuous contact and free of contact configurations essentially differ by the nature of the body force acting on the rod. While solely subjected to its own weight along a contact-free problem, the rod is additionally compelled to lie on the constraint surface along a continuous contact. Assuming frictionless interactions between the rod and the constraint surface, the resulting contact pressure acts as an additional distributed body force oriented normally to the constraint surface, its magnitude being, however, *a priori* unknown.

(b) Governing equations

In the global $\{\boldsymbol{e}_j\}$-basis, the parametrization of the rod centreline is denoted $\boldsymbol{r}(s) = x_j\boldsymbol{e}_j$, where s is referred to as the *Lagrangian coordinate* in contrast with the Eulerian coordinate S. The inextensibility assumption implies that the deformation of the rod leaves invariant the distance between points measured along its centreline. The *material* coordinate s, therefore, identifies a rod cross section independently of the rod configuration. To fully characterize the spatial configuration of the rod, one has to additionally supply this space curve $\mathscr{E}$ with a vector characterizing the orientation of the cross section. Defining a pair of orthonormal vectors $\boldsymbol{d}_1(s)$, $\boldsymbol{d}_2(s)$ along two fixed material lines of the cross section, the rod is entirely defined by the two

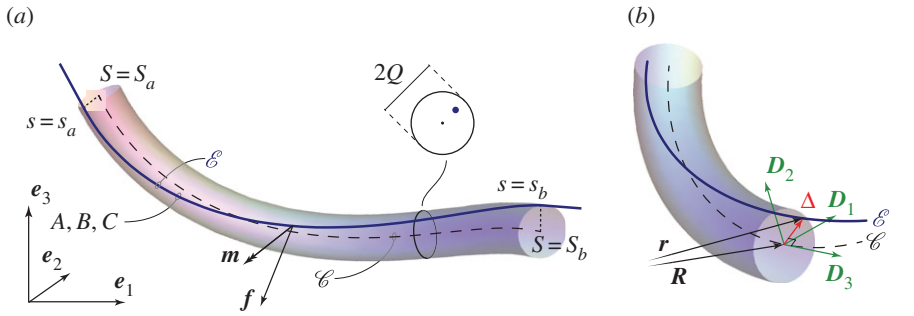

Figure 1. (*a*) Description of the canonical problem: the rod, materialized by its centreline $\mathscr{E}$, is subjected to the body force $\boldsymbol{f}$ and body couple $\boldsymbol{m}$ between its extremities s_a and s_b. It is characterized by its axial stiffness A, bending stiffness B and torsional stiffness C. The constraint is the swept surface generated by a circle of radius Q centred on the reference curve $\mathscr{C}$ and in its normal plane. (*b*) Decomposition of the position vector $\boldsymbol{r}(s(S)) = \boldsymbol{R}(S) + \boldsymbol{\Delta}(S)$ and description of the $\{\boldsymbol{D}_j\}$-basis attached to the reference curve. (Online version in colour.)

vector-valued functions

$$[s_a, s_b] \ni s \mapsto \boldsymbol{r}(s), \boldsymbol{d}_1(s) \in \mathbb{E}^3, \tag{2.1}$$

with $s_a < s_b$ corresponding to the extremities $S_a < S_b$ of the canonical problem (figure 1) and such that the rod length is $\ell = s_b - s_a$. We will henceforth assume that the parametrizations of both the rod centreline and the reference curve are at least C^4-continuous; localized external loads and discontinuous body forces being, therefore, disregarded.

Setting $\boldsymbol{d}_3(s) = \boldsymbol{d}_1 \times \boldsymbol{d}_2$, the triplet of *directors* $\{\boldsymbol{d}_j(s)\}$ constitutes, for each cross section s, a material frame in which the deformed state of the elastic rod is naturally described. While unshearability implies that the normal to the rod cross section is everywhere aligned with the tangent to the rod centreline, *viz.* cross sections remain perpendicular to $\mathscr{E}$, inextensibility expresses that the parametrization $\boldsymbol{r}(s)$ of the rod centreline is arc-length. In other words, the unshearable and inextensible assumptions mean that the director $\boldsymbol{d}_3$ coincides with the tangent vector to the rod centreline

$$\frac{\mathrm{d}\boldsymbol{r}}{\mathrm{d}s} = \boldsymbol{d}_3. \tag{2.2}$$

The kinematic of the directors along the rod satisfies the following skew-symmetric relation

$$\frac{\mathrm{d}\boldsymbol{d}_j}{\mathrm{d}s} = \boldsymbol{u} \times \boldsymbol{d}_j, \tag{2.3}$$

where the twist vector $\boldsymbol{u}(s) = u_j \boldsymbol{d}_j$ relates the rotation of the directors to the strain variables that enter into the constitutive equations: u_1 and u_2 characterize the local material curvatures and u_3 is a kinematic measure of the twist density.

Considering only local interactions between adjacent cross sections of the rod and defining the internal force $\boldsymbol{F}(s) = F_j \boldsymbol{d}_j$ and moment $\boldsymbol{M}(s) = M_j \boldsymbol{d}_j$, the conservation of linear and angular momenta read [24,25, pp. 273–274]

$$\frac{\mathrm{d}\boldsymbol{F}}{\mathrm{d}s} + \boldsymbol{f} = \boldsymbol{0} \tag{2.4}$$

and

$$\frac{\mathrm{d}\boldsymbol{M}}{\mathrm{d}s} + \boldsymbol{d}_3 \times \boldsymbol{F} + \boldsymbol{m} = \boldsymbol{0}, \tag{2.5}$$

where $\boldsymbol{f}(s)$ and $\boldsymbol{m}(s)$ are the body force and body couple per unit reference length at s, respectively. The potential reaction pressure $\boldsymbol{p}(s)$ acting along continuous contacts is treated as an equivalent body force.

For rods with a circular cross section made of a linear elastic material and initially straight, the components of the internal moment are related to the strain variables by means of the following

constitutive equation [26, §2.4]

$$\boldsymbol{M} = B(u_1\boldsymbol{d}_1 + u_2\boldsymbol{d}_2) + Cu_3\boldsymbol{d}_3, \tag{2.6}$$

with the bending stiffness B and the torsional stiffness C. Although the underlying assumption of linear axisymmetric elastic homogeneous constitutive laws has recently be gaining interest in the context of DNA mechanics [27,28], it provides a reasonably good estimate for a wide range of applications without overcomplicating the presentation of the proposed formulation.

(c) Discussion: boundary conditions and unilateral contact condition

Classic boundary-value problems for $\{\boldsymbol{r}(s), \boldsymbol{d}_1(s)\}$ consist of the kinematic equations (2.2)–(2.3), the equilibrium equations (2.4) and (2.5), the constitutive relation (2.6) and a combination of kinematic and mechanical boundary conditions [25, pp. 322–328]. Considering the orthonormality of the directors, the resulting system consists of 15 first-order differential equations which requires a set of 15 boundary conditions. For an exhaustive description of the various families and possible combinations of boundary conditions associated with elastic rods, see [29, pp. 297–300]. The regular boundary-value problems associated with a fixed length $\ell = s_b - s_a$ have been investigated from various perspectives and closed form solutions have been obtained under particular sets of boundary conditions and loadings [30–32]. These configurations can, however, be regarded as exceptional and one must generally resort to numerical techniques [28,33,34] to solve the general problem.

In the context under consideration, one extremity of the rod is clamped while the other moves freely through a frictionless sliding sleeve under the combined action of known axial force and twisting moment. One may assume, without loss of generality, the extremity s_a to be clamped such that the triplet

$$\{\boldsymbol{r}(s_a), \boldsymbol{d}_1(s_a), \boldsymbol{d}_2(s_a)\} \tag{2.7}$$

is prescribed at this point. At the end s_b of the boundary-value problem, the position of the rod and the unit tangent are imposed together with the axial force and twisting moment, i.e.

$$\{\boldsymbol{r}(s_b), \boldsymbol{d}_3(s_b), F_3(s_b), M_3(s_b)\}. \tag{2.8}$$

The rod length $\ell = s_b - s_a$ being unknown, the resulting free boundary problem is well posed. The boundary conditions specifying the locations $\boldsymbol{r}(s_a)$ and $\boldsymbol{r}(s_b)$ of the rod centreline at both extremities of the domain, however, lead to the establishment of isoperimetric constraints. Indeed, although the rod spatial configuration has been specified through the position vector of the rod centreline and the director $\boldsymbol{d}_1(s)$, the parametrization $\boldsymbol{r}(s)$ of the space curve $\mathscr{E}$ does not explicitly appear in the governing equations. The coordinates $x_j(s)$ of the rod centreline in the absolute reference frame $\{\boldsymbol{e}_j\}$, therefore, require the integration of the kinematic relation (2.2), that is

$$x_j(s) = x_j(s_a) + \int_{s_a}^{s} \boldsymbol{d}_3 \cdot \boldsymbol{e}_j \, \mathrm{d}s. \tag{2.9}$$

Within the conventional Lagrangian formulation, the resolution of the free boundary problem associated with this set of integral constraints on the unknown domain $[s_a, s_b]$ requires the use of involved numerical techniques, e.g. adapted shooting methods [35] or the tau method [36], which contribute to the numerical burden of this approach.

As noted in Introduction, the assessment of the unilateral contact condition constitutes an additional source of difficulties. To ensure that the rod remains either in continuous contact or free of contact along the whole domain of the problem under consideration, this supplementary constraint necessitates the evaluation of the distance between the rod centreline $\mathscr{E}$ and the reference curve $\mathscr{C}$. However, these two curves being naturally parametrized by the Lagrangian and Eulerian curvilinear coordinates, s and S, respectively, the evaluation of this distance reveals to be computationally intensive as it requires the identification of the mapping $s \mapsto S(s)$, from Lagrangian to Eulerian coordinates.

Finally, the ill-conditioning of the governing equations for small bending stiffness, the existence of spurious solutions associated with curling of the rod as well as the demand for increasing accuracy of the solutions with decreasing clearance, are sources of various additional complications or other bottlenecks. Consequently, the Lagrangian formulation of the problem is ineffective and laborious to solve in some circumstances [22].

3. Eulerian formulation

The proposed reformulation hinges on describing the rod-deformed configuration by means of its relative position about the reference curve and restating the rod local equilibrium in terms of the Eulerian curvilinear coordinate associated with $\mathscr{C}$ rather than the natural Lagrangian coordinate of the rod. The objective of this re-parametrization of the problem is twofold: (i) transform the free boundary problem, associated with isoperimetric constraints on an unknown domain, into a conventional two-point boundary-value problem and (ii) trivialize the detection of new contacts.

By analogy with the director basis, one may arbitrarily define a triplet $\{\boldsymbol{D}_j(S)\}$ constituting a right-handed orthonormal basis for each cross section S along the reference curve and such that $\boldsymbol{D}_3 = \mathrm{d}\boldsymbol{R}/\mathrm{d}S$ is the unit vector tangent to $\mathscr{C}$. The kinematics of this adapted frame along the reference curve can, therefore, be described by means of a vector $\boldsymbol{U}(S) = U_j\boldsymbol{D}_j$ [37] as

$$\frac{\mathrm{d}\boldsymbol{D}_j}{\mathrm{d}S} = \boldsymbol{U} \times \boldsymbol{D}_j. \tag{3.1}$$

Although theoretically appealing, the identification of this frame with the Frenet–Serret apparatus attached to $\mathscr{C}$ may lead to existence and continuity issues for reference curves with vanishing curvature. While it is not a requisite for the present formulation, defining the $\{\boldsymbol{D}_j\}$—basis such that it constitutes a Bishop frame [38] is advocated as it results in substantially simpler expressions. Also referred to as the parallel transport frame, this adapted frame constitutes an alternative approach to defining a moving frame that is everywhere well defined. Its construction is based on the concept of relatively parallel fields and the observation that, while the tangent vector $\boldsymbol{D}_3$ is unique for any given curve, the pair of orthonormal vectors $\{\boldsymbol{D}_1, \boldsymbol{D}_2\}$ may be chosen arbitrarily provided it remains perpendicular to the tangent vector. In particular, the pair $\{\boldsymbol{D}_1, \boldsymbol{D}_2\}$ may be defined such that the $\{\boldsymbol{D}_j\}$-basis smoothly varies along $\mathscr{C}$ and has zero twist uniformly, i.e. $U_3(S) = 0$, by requiring $\mathrm{d}\boldsymbol{D}_1/\mathrm{d}S \cdot \boldsymbol{D}_2 = 0$ and $\mathrm{d}\boldsymbol{D}_2/\mathrm{d}S \cdot \boldsymbol{D}_1 = 0$.

As presented in figure 1*b*, the position vector for the rod cross section centroid $\boldsymbol{r}(s) = x_j\boldsymbol{e}_j$ can, naturally, be expressed as

$$\boldsymbol{r}(s(S)) = \boldsymbol{R}(S) + \boldsymbol{\Delta}(S), \tag{3.2}$$

where the *eccentricity vector* $\boldsymbol{\Delta}(S) = \Delta_1\boldsymbol{D}_1 + \Delta_2\boldsymbol{D}_2$ is a measure of the rod relative position in the cross section of abscissa S. Besides describing the space curve $\mathscr{E}$ with respect to the reference curve $\mathscr{C}$, this decomposition of the position vector $\boldsymbol{r}(s)$ connects the Eulerian and Lagrangian formulations through the mapping $S \mapsto s(S)$.

In the following, derivatives of scalar- and vector-valued functions with respect to the Eulerian coordinate S will be denoted by the apposition of a prime while derivatives with respect to the Lagrangian coordinate s are explicitly specified.

(a) Mapping and Jacobian

The reformulation of the local equilibrium (2.4)–(2.5) within the Eulerian framework requires to express the natural derivatives $\mathrm{d}\cdot/\mathrm{d}s$ in terms of Eulerian derivatives $\mathrm{d}\cdot/\mathrm{d}S$. The Jacobian of the mapping $S \mapsto s(S)$, from Eulerian to Lagrangian coordinates, is obtained by inserting the decomposition (3.2) of the rod centreline in equation (2.2) and applying the chain rule differentiation

$$s'(S) = \pm\|\boldsymbol{D}_3 + \boldsymbol{\Delta}'\|. \tag{3.3}$$

As $\boldsymbol{D}_3$ is a unit vector, the drift between the two curvilinear coordinates is caused by the eccentricity $\boldsymbol{\Delta}$ between the rod and the reference curve. Opting for either the positive or negative

sign in this expression, *viz.* imposing the mapping $s(S)$ to be injective, prevents the appearance of solutions associated with curling, writhing or other configurations involving self-contact. Considered unlikely to occur in the present context, these solutions are disregarded. Also the positive sign in expression (3.3) is selected.

Similarly, the derivatives of the inverse mapping $s \mapsto S(s)$, from Lagrangian to Eulerian coordinates, can be explicitly written in terms of the Eulerian functions $\Delta_i(S)$ and $U_j(S)$ (with $i = 1, 2$ and $j = 1, 2, 3$.) Defining the Eulerian function $J_k(S)$ as

$$J_k(S) = \left.\frac{\mathrm{d}^k S}{\mathrm{d}s^k}\right|_{s=s(S)}, \tag{3.4}$$

with $J_1(S) = 1/s'(S)$, the recursive relation

$$J_k(S) = J'_{k-1} J_1 \tag{3.5}$$

is obtained for $k > 1$.

(b) Directors and strain variables

Through the introduction of the eccentricity vector, the space curve $\mathscr{E}$ characterizing the rod centreline in its deformed configuration is expressed by reference to the space curve $\mathscr{C}$. Differentiating (3.2) with respect to the Eulerian coordinate, the rod local inclination reads

$$\boldsymbol{d}_3 = J_1(\boldsymbol{D}_3 + \boldsymbol{\Delta}'), \tag{3.6}$$

which emphasizes its representation in terms of the tangent vector to the reference curve. Projecting this relation in the $\{\boldsymbol{D}_j\}$-basis and accounting for the definition (3.1) of the vector $\boldsymbol{U}(S)$, the components of $\boldsymbol{d}_3$ in the frame attached to the reference curve are

$$g_1(S) = \boldsymbol{d}_3 \cdot \boldsymbol{D}_1 = J_1(\Delta'_1 - \Delta_2 U_3), \tag{3.7}$$

$$g_2(S) = \boldsymbol{d}_3 \cdot \boldsymbol{D}_2 = J_1(\Delta'_2 + \Delta_1 U_3) \tag{3.8}$$

and

$$g_3(S) = \boldsymbol{d}_3 \cdot \boldsymbol{D}_3 = J_1(1 - \Delta_1 U_2 + \Delta_2 U_1), \tag{3.9}$$

with $g_1^2 + g_2^2 + g_3^2 = 1$. Provided the $\{\boldsymbol{D}_j\}$'s be defined such that they constitute a Bishop frame, the former two expressions considerably simplify as $U_3(S) = 0$.

The attitude of the rod cross section being uniquely defined by the director $\boldsymbol{d}_3$, the knowledge of the angle between either director $\boldsymbol{d}_1$ or $\boldsymbol{d}_2$ and a specified direction is sufficient to fully characterize the rod spatial configuration. Although straightforward, the characterization of this rotation with respect to the normal and binormal to the space curve $\mathscr{E}$ may lead to uniqueness and continuity issues as the Frenet–Serret apparatus ceases to be defined at inflection points [39, pp. 46–50], *viz.* where the rod curvature κ vanishes. Alternatively, as depicted in figure 2, the rotation of the rod cross section about the director $\boldsymbol{d}_3$ can be described with respect to the pair $\{\boldsymbol{k}_1, \boldsymbol{k}_2\}$

$$\boldsymbol{d}_1 = \cos\varphi \boldsymbol{k}_1 + \sin\varphi \boldsymbol{k}_2 \tag{3.10}$$

and

$$\boldsymbol{d}_2 = -\sin\varphi \boldsymbol{k}_1 + \cos\varphi \boldsymbol{k}_2, \tag{3.11}$$

where the unit vectors $\boldsymbol{k}_1$ and $\boldsymbol{k}_2$ are the images of $\boldsymbol{D}_1$ and $\boldsymbol{D}_2$, respectively, through the rotation mapping $\boldsymbol{D}_3$ on $\boldsymbol{d}_3$. Rodrigues formula [40] yields

$$\boldsymbol{k}_j = \boldsymbol{D}_j + \boldsymbol{\vartheta} \times \boldsymbol{D}_j + \frac{\boldsymbol{\vartheta} \times (\boldsymbol{\vartheta} \times \boldsymbol{D}_j)}{(1 + \cos\theta)}, \tag{3.12}$$

where $\cos\theta = g_3$ and $\boldsymbol{\vartheta} = \boldsymbol{D}_3 \times \boldsymbol{d}_3$, with $\|\boldsymbol{\vartheta}\| = \sin\theta$, is the vector describing the axis of rotation. Additionally, defining $\boldsymbol{k}_3 = \boldsymbol{d}_3$, the triplet $\{\boldsymbol{k}_j\}$ constitutes a right-handed orthonormal basis that coincides with the directors for $\cos\varphi = 1$ and degenerates into the $\boldsymbol{D}_j$-basis for $\cos\theta = 1$, i.e. for $\boldsymbol{\vartheta} = \boldsymbol{0}$. Entirely defined by the three Eulerian functions g_j (see appendix A), this *intermediate* basis

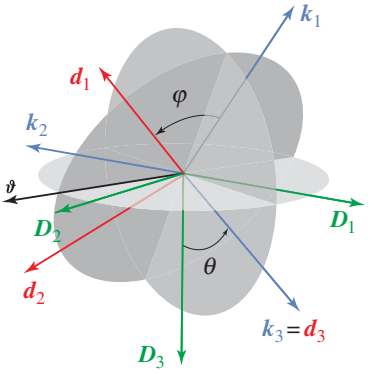

Figure 2. Definition of the angle φ and description of the $\{\boldsymbol{k}_j\}$-basis as the images of the $\{\boldsymbol{D}_j\}$-basis through the rotation about $\boldsymbol{\vartheta} = \boldsymbol{D}_3 \times \boldsymbol{d}_3$ and mapping $\boldsymbol{D}_3$ on $\boldsymbol{d}_3$. (Online version in colour.)

attached to $\mathscr{C}$ provides a simple way to describe the orientation of the directors with respect to the known $\{\boldsymbol{D}_j\}$-basis as well as the rudiments to re-express the strain variables in terms of Eulerian functions. Henceforth, tildes will be used to distinguish components of vectorial quantities in the $\{\boldsymbol{k}_j\}$-basis from their counterpart in the directors basis, e.g. $u_j = \boldsymbol{u} \cdot \boldsymbol{d}_j$ and $\tilde{u}_j = \boldsymbol{u} \cdot \boldsymbol{k}_j$.

Analogous to relation (2.3) for the directors, the kinematic of the intermediate $\{\boldsymbol{k}_j\}$-basis along the rod centreline is described by a *fictitious* twist vector $\boldsymbol{w} = \tilde{w}_j \boldsymbol{k}_j$ defined such that

$$\frac{\mathrm{d}\boldsymbol{k}_j}{\mathrm{d}s} = \boldsymbol{w} \times \boldsymbol{k}_j \tag{3.13}$$

and which differs from the actual twist vector $\boldsymbol{u}$ as a result of the relative rotation φ of the directors $\{\boldsymbol{d}_1, \boldsymbol{d}_2\}$ with respect to the pair $\{\boldsymbol{k}_1, \boldsymbol{k}_2\}$. Hence, in view of the kinematic relations (2.3) and (3.13), differentiation of expressions (3.10)–(3.11) leads to $\boldsymbol{u} = \boldsymbol{w} + J_1\varphi'\boldsymbol{d}_3$ for the twist vector and

$$u_1(S) = \tilde{w}_1 \cos\varphi + \tilde{w}_2 \sin\varphi, \tag{3.14}$$

$$u_2(S) = -\tilde{w}_1 \sin\varphi + \tilde{w}_2 \cos\varphi \tag{3.15}$$

and

$$u_3(S) = \tilde{w}_3 + J_1\varphi', \tag{3.16}$$

for the strain variables. The components $\tilde{w}_1(S)$ and $\tilde{w}_2(S)$ are the projections of $\mathrm{d}\boldsymbol{d}_3/\mathrm{d}s = \kappa\boldsymbol{n}$ on $\boldsymbol{k}_1$ and $\boldsymbol{k}_2$, respectively, while $\tilde{w}_3(S) = w_3$ may be interpreted as the twist density associated with the rotation of the pair $\{\boldsymbol{k}_1, \boldsymbol{k}_2\}$ about $\boldsymbol{k}_3$. Their expressions, in terms of the Eulerian quantities, are obtained by substituting the definition (3.12) for the $\boldsymbol{k}_j$'s in the projection of equation (3.13) on the $\{\boldsymbol{k}_j\}$-basis

$$\tilde{w}_1(S) = \frac{\mathrm{d}\boldsymbol{k}_2}{\mathrm{d}s} \cdot \boldsymbol{k}_3 = J_1\left(\tilde{U}_1 - g_2' + \frac{g_2 g_3'}{1+g_3}\right), \tag{3.17}$$

$$\tilde{w}_2(S) = \frac{\mathrm{d}\boldsymbol{k}_3}{\mathrm{d}s} \cdot \boldsymbol{k}_1 = J_1\left(\tilde{U}_2 + g_1' - \frac{g_1 g_3'}{1+g_3}\right) \tag{3.18}$$

and

$$\tilde{w}_3(S) = \frac{\mathrm{d}\boldsymbol{k}_1}{\mathrm{d}s} \cdot \boldsymbol{k}_2 = J_1\left(\tilde{U}_3 - \frac{g_1 g_2' - g_1' g_2}{1+g_3}\right). \tag{3.19}$$

These relations emphasize that the kinematics of the $\{\boldsymbol{k}_j\}$-basis may be decomposed into the kinematics of the $\{\boldsymbol{D}_j\}$-basis, characterized by the Darboux vector $\boldsymbol{U}(S)$, and its rotation with

respect to this basis. The components $\tilde{U}_j(S)$ of $\boldsymbol{U}(S)$ in the $\{\boldsymbol{k}_j\}$-basis are given in appendix A in terms of the g_j's and U_j's.

In conclusion, through substitution of equations (3.10)–(3.11) and (3.14)–(3.16), the constitutive law (2.6) reads

$$\boldsymbol{M}(S) = B(\tilde{w}_1\boldsymbol{k}_1 + \tilde{w}_2\boldsymbol{k}_2) + C(\tilde{w}_3 + J_1\varphi')\boldsymbol{k}_3, \tag{3.20}$$

where, according to equations (3.17)–(3.19), the $\tilde{w}_j(S)$ are given in terms of the $g_j(S)$ defined in equations (3.7)–(3.9). Provided that the body force and body couple per unit reference length may be expressed as functions of the Eulerian curvilinear coordinate, *viz.* $\boldsymbol{f}(S) = \boldsymbol{f}(S(s))$ and $\boldsymbol{m}(S) = \boldsymbol{m}(S(s))$, the balance of linear and angular momenta (2.4)–(2.5) may be expressed as

$$J_1\frac{\mathrm{d}\boldsymbol{F}}{\mathrm{d}S} + \boldsymbol{f} = \boldsymbol{0} \tag{3.21}$$

and

$$J_1\frac{\mathrm{d}\boldsymbol{M}}{\mathrm{d}S} + \boldsymbol{k}_3 \times \boldsymbol{F} + \boldsymbol{m} = \boldsymbol{0}, \tag{3.22}$$

where, according to relations (3.3) and (3.4), the Jacobian reads

$$J_1(S) = \frac{1}{\sqrt{(\Delta_1' - \Delta_2 U_3)^2 + (\Delta_2' + \Delta_1 U_3)^2 + (1 - \Delta_1 U_2 + \Delta_2 U_1)^2}}, \tag{3.23}$$

which completes the Eulerian formulation.

(c) Governing equations and boundary conditions

Both the Eulerian coordinate S and the components of the eccentricity vector are scaled by the known length of the boundary-value problem, $L = S_b - S_a$, leading to the introduction of the dimensionless curvilinear coordinate $\xi = (S - S_a)/L$ and eccentricity vector $\boldsymbol{\delta}(\xi) = \delta_1\boldsymbol{D}_1 + \delta_2\boldsymbol{D}_2$ with

$$\delta_1(\xi) = \frac{\Delta_1(S(\xi))}{L} \quad \text{and} \quad \delta_2(\xi) = \frac{\Delta_2(S(\xi))}{L}. \tag{3.24}$$

Analogously scaling the Lagrangian coordinate by L, the Jacobians derivatives (3.6) read

$$\mathcal{J}_k(\xi) = L^{k-1}J_k(S(\xi)), \tag{3.25}$$

for $k \geq 1$. Similarly, the fictitious twist vector and the Darboux vector scale as

$$\boldsymbol{\omega}(\xi) = L\boldsymbol{w}(S(\xi)) \quad \text{and} \quad \mathcal{U}(\xi) = L\boldsymbol{U}(S(\xi)), \tag{3.26}$$

such that the Jacobian (3.23) reads

$$\mathcal{J}_1(\xi) = \frac{1}{\sqrt{(\delta_1' - \delta_2\mathcal{U}_3)^2 + (\delta_2' + \delta_1\mathcal{U}_3)^2 + (1 - \delta_1\mathcal{U}_2 + \delta_2\mathcal{U}_1)^2}}, \tag{3.27}$$

where primes now denote differentiation with respect to the dimensionless coordinate ξ.

Considering the previous definitions and denoting the characteristic force $F^\star = B/L^2$, the scaling leads to the introduction of the following vector fields

$$\boldsymbol{\mathcal{F}}(\xi) = \frac{\boldsymbol{F}(S(\xi))}{F^\star}, \quad \boldsymbol{\mathcal{M}}(\xi) = \frac{\boldsymbol{M}(S(\xi))}{LF^\star}, \tag{3.28}$$

and

$$\boldsymbol{\sigma}(\xi) = \frac{L\boldsymbol{f}(S(\xi))}{F^\star}, \quad \boldsymbol{\mu}(\xi) = \frac{\boldsymbol{m}(S(\xi))}{F^\star}, \tag{3.29}$$

for the scaled internal force and moment, body force and body couple, respectively. According to this scaling and the constitutive relation (2.6), the dimensionless strain variables are analogous to

the components of the scaled internal moment in the directors basis, that is

$$\mathcal{M}_1(\xi) = Lu_1, \quad \mathcal{M}_2(\xi) = Lu_2 \quad \text{and} \quad \mathcal{M}_3(\xi) = Lu_3(1+\nu)^{-1}, \tag{3.30}$$

where, for rods with a circular cross section, $\nu = B/C - 1$ is Poisson's ratio. Relation (3.20), therefore, becomes

$$\boldsymbol{\mathcal{M}}(\xi) = \tilde{\omega}_1 \boldsymbol{k}_1 + \tilde{\omega}_2 \boldsymbol{k}_2 + (1+\nu)^{-1}(\tilde{\omega}_3 + J_1\varphi')\boldsymbol{k}_3, \tag{3.31}$$

where $\varphi(\xi) = \varphi(S(\xi))$. The projection of the equilibrium equations (3.21)–(3.22) in the $\{\boldsymbol{k}_j\}$-basis then yields

$$\mathcal{J}_1\tilde{\mathcal{F}}_1' + \tilde{\omega}_2\tilde{\mathcal{F}}_3 - \tilde{\omega}_3\tilde{\mathcal{F}}_2 + \tilde{\sigma}_1 = 0, \tag{3.32}$$

$$\mathcal{J}_1\tilde{\mathcal{F}}_2' + \tilde{\omega}_3\tilde{\mathcal{F}}_1 - \tilde{\omega}_1\tilde{\mathcal{F}}_3 + \tilde{\sigma}_2 = 0, \tag{3.33}$$

$$\mathcal{J}_1\tilde{\mathcal{F}}_3' + \tilde{\omega}_1\tilde{\mathcal{F}}_2 - \tilde{\omega}_2\tilde{\mathcal{F}}_1 + \tilde{\sigma}_3 = 0, \tag{3.34}$$

$$\mathcal{J}_1\tilde{\omega}_1' - \frac{\tilde{\omega}_2}{1+\nu}(\nu\tilde{\omega}_3 - \mathcal{J}_1\varphi') - \tilde{\mathcal{F}}_2 + \tilde{\mu}_1 = 0, \tag{3.35}$$

$$\mathcal{J}_1\tilde{\omega}_2' + \frac{\tilde{\omega}_1}{1+\nu}(\nu\tilde{\omega}_3 - \mathcal{J}_1\varphi') + \tilde{\mathcal{F}}_1 + \tilde{\mu}_2 = 0 \tag{3.36}$$

and

$$\mathcal{J}_1^2\varphi'' + \mathcal{J}_2\varphi' + \mathcal{J}_1\tilde{\omega}_3' + (1+\nu)\tilde{\mu}_3 = 0, \tag{3.37}$$

with $\tilde{\mathcal{F}}_j(\xi) = \boldsymbol{\mathcal{F}} \cdot \boldsymbol{k}_j$, $\tilde{\sigma}_j(\xi) = \boldsymbol{\sigma} \cdot \boldsymbol{k}_j$ and $\tilde{\mu}_j(\xi) = \boldsymbol{\mu} \cdot \boldsymbol{k}_j$, and where the components (3.17)–(3.19) of the fictitious twist vector $\boldsymbol{\omega}(\xi)$ in the intermediate basis read

$$\tilde{\omega}_1(\xi) = \mathcal{J}_1\left(\tilde{\mathcal{U}}_1 - g_2' + \frac{g_2 g_3'}{1+g_3}\right), \tag{3.38}$$

$$\tilde{\omega}_2(\xi) = \mathcal{J}_1\left(\tilde{\mathcal{U}}_2 + g_1' - \frac{g_1 g_3'}{1+g_3}\right) \tag{3.39}$$

and

$$\tilde{\omega}_3(\xi) = \mathcal{J}_1\left(\tilde{\mathcal{U}}_3 - \frac{g_1 g_2' - g_1' g_2}{1+g_3}\right), \tag{3.40}$$

with the components (3.7)–(3.9) of the unit tangent $\boldsymbol{d}_3$ in the $\{\boldsymbol{D}_j\}$-basis given by

$$g_1(\xi) = \mathcal{J}_1(\delta_1' - \delta_2\mathcal{U}_3), \tag{3.41}$$

$$g_2(\xi) = \mathcal{J}_1(\delta_2' + \delta_1\mathcal{U}_3) \tag{3.42}$$

and

$$g_3(\xi) = \mathcal{J}_1(1 - \delta_1\mathcal{U}_2 + \delta_2\mathcal{U}_1), \tag{3.43}$$

with the Jacobian $\mathcal{J}_1(\xi)$ as defined in equations (3.27).

The six differential equations (3.32)–(3.37) with expression (3.27) for the Jacobian $\mathcal{J}_1$ and the definitions (3.38)–(3.43) for the $\tilde{\omega}_j$'s and the g_j's result in an 11th order system of nonlinear differential equations in the six Eulerian unknowns $\{\varphi, \delta_1, \delta_2, \tilde{\mathcal{F}}_1, \tilde{\mathcal{F}}_2, \tilde{\mathcal{F}}_3\}$. For the sake of readability, this mixed order system is given in the electronic supplementary material. These governing equations, whose structures are conserved in the small inclination approximation presented in appendix B, involve three first-order differential equation, (3.32)–(3.34), in the $\tilde{\mathcal{F}}_j$'s; one second-order, (3.37), in φ and two third-order, (3.35)–(3.36), in the δ_i's (with $i = 1, 2$ and $j = 1, 2, 3$.)

This mixed-order system consequently requires the specification of 11 constants of integration. The Eulerian counterpart to the boundary conditions (2.7) prescribing the clamped extremity of the rod reads

$$\{\varphi(0), \delta_i(0), \delta_i'(0)\}, \tag{3.44}$$

with $i = 1, 2$. At the end S_b of the boundary-value problem, the rod remains free to move smoothly through a frictionless sliding sleeve, whose position is fixed in space. Both eccentricity and inclination of the rod with respect to the reference curve must, therefore, be imposed. Additionally, according to the constitutive relations (3.31), the known twisting moment acting

at this extremity also requires to prescribe the first derivative of the angle φ. Hence, the boundary conditions (2.8) becomes

$$\{\varphi'(1), \delta_i(1), \delta_i'(1), \tilde{\mathcal{F}}_3(1)\}, \tag{3.45}$$

with $i = 1, 2$. As an essential outcome of the proposed reformulation, the isoperimetric constraints on the unknown length of the rod, a source of difficulty in the Lagrangian formulation, disappear and the system of equations (3.32)–(3.37) with the boundary conditions (3.44))–(3.45) constitute a classical boundary-value problem (as opposed to a free boundary problem.) Note that the proposed Eulerian reformulation of the rod-governing equations could be extended to other boundary conditions.

In conclusion, it has been shown that the rod configuration, entirely defined by $\boldsymbol{r}(s)$ and $\boldsymbol{d}_1(s)$ in the Lagrangian formulation (2.1), reduces to the knowledge of the three Eulerian functions

$$[0, 1] \ni \xi \mapsto \varphi(\xi), \delta_1(\xi), \delta_2(\xi) \in \mathbb{R}, \tag{3.46}$$

with the boundaries $\xi = \{0, 1\}$ of the canonical problem corresponding to the rod extremities s_a and s_b, respectively. While the components δ_1, δ_2 of the eccentricity vector describe the rod relative position with respect to the reference curve, the angle φ characterizes the rotation of the rod cross section about the director $\boldsymbol{d}_3$. This representation of elastic rods leads to a reduced coordinate formulation involving a minimal number of degrees of freedom similar to the *curve-angle* representations proposed in [33,41–43]. In this formulation, the centreline is explicitly represented and the material frame is characterized by a unique angle.

Besides the suppression of the isoperimetric constraints, the proposed Eulerian reformulation of the rod-governing equations drastically simplifies the assessment of the unilateral contact condition, which requires the evaluation of the distance between the two curves $\mathscr{C}$ and $\mathscr{E}$ (parametrized by distinct curvilinear coordinates in the classical Lagrangian formulation.) Specifically, the description of the rod's deformed configuration through its relative position with respect to the constraint axis provides a straightforward means to detect the appearance of new contacts or, depending on the elementary problem under consideration, ensuring that the rod remains in continuous contact with the constraining surface. More precisely:

(i) Free rod

The *a posteriori* assessment of the unilateral contact condition along contact-free problems is drastically simplified as it reduces to ensuring that a threshold on the magnitude of the eccentricity vector is not violated. This constraint, indeed, merely consists in checking that either $\|\boldsymbol{\delta}\| < \epsilon$ or $\|\boldsymbol{\delta}\| > \epsilon$, with the scaled constraint radius $\epsilon(\xi) = Q(S(\xi))/L$, for interior and exterior configurations, respectively.

(ii) Continuous contact

Alternatively, although the magnitude of the eccentricity vector is known along continuous contact problems, the magnitude of the reaction pressure $\boldsymbol{\rho}(\xi)$ included in the body force $\boldsymbol{\sigma}(\xi)$ and acting normally to the constraint surface is *a priori* unknown. The nonlinear boundary-value problem (3.32)–(3.45) is, therefore, supplemented by the relation $\|\boldsymbol{\delta}\| = \epsilon$ to close the formulation and ensure the continuous contact along the whole domain. As emphasized in [42,44], one may always recombine equations (3.32)–(3.33) and (3.35)–(3.36) to eliminate the algebraic component, *viz.* the reaction pressure, from the resulting system of differential-algebraic equations. This approach, illustrated in §4b for the continuous contact with a cylindrical constraint, is equivalent to projecting the governing equations (3.21)–(3.22) along the normal and geodesic directions to the constraint surface, allowing to reduce the system to a set of ordinary differential equations.

4. Validation and applications

As suggested in Introduction, the range of disciplines and applications concerned with the constrained deformation of a slender elastic body is potentially very wide. Exploring all the

possible features of the proposed Eulerian reformulation exceeds the scope of this paper and, merely, a few of its benefits and limitations are highlighted in the following. Considering a series of elementary problems, the validity of the method is assessed by comparison with known analytical results and numerical solutions obtained using the Lagrangian formulation.

(a) Planar elastica

Planar deflection can either result from the rod cross section geometry and loading symmetry (these solutions do not need to be stable) or be imposed by external constraints (in which case the transversal force is not necessarily null). The purely bi-dimensional configuration corresponding to the external constraint $\boldsymbol{d}_2(\xi) = \boldsymbol{e}_2$ is investigated here by assuming $\delta_2(\xi) = 0$ and a planar reference curve. The $\{\boldsymbol{D}_j\}$-basis attached to $\mathscr{C}$ is defined such that $\boldsymbol{D}_2(\xi) = \boldsymbol{e}_2$; hence, the only non-null component of the Darboux vector $\mathcal{U}(\xi) = \mathcal{U}_2\boldsymbol{D}_2$ corresponds to the curvature of the reference curve.

Consequently, the components of the director $\boldsymbol{d}_3$ in the frame attached to the reference curve, cf. equations (3.41)–(3.43), reduce to

$$g_1(\xi) = \mathcal{J}_1\delta_1', \quad g_2(\xi) = 0 \quad \text{and} \quad g_3(\xi) = \mathcal{J}_1(1 - \delta_1\mathcal{U}_2), \tag{4.1}$$

where, according to equation (3.27), the Jacobian from Eulerian to stretched coordinates is given by

$$\mathcal{J}_1(\xi) = \frac{1}{\sqrt{\delta_1'^2 + (1 - \delta_1\mathcal{U}_2)}}. \tag{4.2}$$

The only non-null component of the fictitious twist vector (3.38)–(3.40), therefore, reads

$$\tilde{\omega}_2(\xi) = \tilde{\mathcal{J}}_1^3(\mathcal{U}_2 + \delta_1'' - 2\delta_1\mathcal{U}_2^2 + \delta_1^2\mathcal{U}_2^3 + 2\delta_1'^2\mathcal{U}_2 - \delta_1\delta_1''\mathcal{U}_2 - \delta_1\delta_1'\mathcal{U}_2'), \tag{4.3}$$

which is the curvature of the rod. Hence, according to equations (3.14)–(3.16) and (3.30), the strain variables reduce to

$$\mathcal{M}_1 = \tilde{\omega}_2 \sin\varphi, \quad \mathcal{M}_2 = \tilde{\omega}_2 \cos\varphi \quad \text{and} \quad \mathcal{M}_3 = \mathcal{J}_1\frac{\varphi'}{1+\nu}. \tag{4.4}$$

Assuming no rotation of the rod cross section about its axis, i.e. $\varphi'(\xi) = 0$, the Eulerian formulation proposed by [22] for a constrained elastica is recovered.

(b) Straight conduit

The helical buckling and post-buckling behaviour of a rod within a cylindrical constraint has been studied extensively [45–50] not only due to the major interest it represents to several areas of science and engineering (e.g. mechanics of climbing in twining plants, drilling industry, fittings in overhead transmission lines or buckling of optical fibres in loose-tube packaging), but also as a result of the position this fundamental problem occupies in advanced continuum mechanics. Here, it is shown that well-known results associated with twisted elastic rods can easily be recovered from the proposed Eulerian formulation of the rod-governing equations.

Along a straight reference curve framed by a constant $\{\boldsymbol{D}_j\}$-basis, the rod assumes a helical deflection with radius $\delta = \|\boldsymbol{\delta}\|$ and pitch angle θ provided the components of the eccentricity vector satisfy

$$\delta_1(\xi) = \delta\cos\left(\frac{2\pi\xi}{\lambda}\right) \quad \text{and} \quad \delta_2(\xi) = \delta\sin\left(\frac{2\pi\xi}{\lambda}\right), \tag{4.5}$$

where $\lambda = 2\pi\delta/\tan\theta$ is the helix axial wavelength or pitch. Note that the pitch angle θ is also the inclination of the rod on the reference curve as defined in equation (3.12). The Jacobian of the mapping from Eulerian to Lagrangian coordinates reduces then to $\mathcal{J}_1(\xi) = \cos\theta$ and, restricting ourselves to weightless rods and frictionless contact, the reaction pressure $\boldsymbol{\rho}(\xi)$ is equivalent to a body force acting normally to the constraint surface, i.e. $\boldsymbol{\rho}\cdot\boldsymbol{D}_3 = 0$.

In this context, it may be convenient to decompose the shear forces into their normal $\mathcal{F}_\mathrm{n}$ and geodesic $\mathcal{F}_\mathrm{g}$ components, that is their normal and tangential components with respect to the cylindrical constraining surface. This decomposition reads

$$\mathcal{F}_1(\xi) = \mathcal{F}_\mathrm{n} \cos\left(\frac{2\pi\xi}{\lambda}\right) - \mathcal{F}_\mathrm{g} \sin\left(\frac{2\pi\xi}{\lambda}\right) \tag{4.6}$$

and

$$\mathcal{F}_2(\xi) = \mathcal{F}_\mathrm{n} \sin\left(\frac{2\pi\xi}{\lambda}\right) + \mathcal{F}_\mathrm{g} \cos\left(\frac{2\pi\xi}{\lambda}\right), \tag{4.7}$$

with $\mathcal{F}_\mathrm{n} = \mathcal{F}\cdot\boldsymbol{N}$ and $\mathcal{F}_\mathrm{g} = \mathcal{F}\cdot(\boldsymbol{N}\times\boldsymbol{d}_3)$, where $\boldsymbol{N}(\xi) = \cos(2\pi\xi/\lambda)\boldsymbol{D}_1 + \sin(2\pi\xi/\lambda)\boldsymbol{D}_2$. Hence, substituting expressions (4.5) for δ_1 and δ_2 in the equilibrium equations (3.35) and (3.36) leads to

$$\mathcal{F}_\mathrm{n}(\xi) = 0 \tag{4.8}$$

and

$$\mathcal{F}_\mathrm{g}(\xi) = \frac{\cos\theta\sin^2\theta}{(1+\nu)\delta^2}[\tan\theta(1+\nu\cos\theta) - \delta\varphi']. \tag{4.9}$$

Considering solutions homoclinic to the straight unbuckled configuration (i.e. asymptotically straight towards both ends), the applied end twisting moment $\mathcal{M} = \boldsymbol{\mathcal{M}}\cdot\boldsymbol{D}_3$ is carried about the rod material axis such that the constant torque reads $\mathcal{M}_3 = \mathcal{M}$ [48,51,52]. According to equations (3.34) and (3.37), the axial component of the internal force $\mathcal{F}_3$ and the angle φ then read

$$\mathcal{F}_3(\xi) = \left(\mathcal{T} - \frac{\sin^4\theta}{\delta^2}\right)\sec\theta \tag{4.10}$$

and

$$\varphi(\xi) = \varphi(0) + \xi\,\frac{\tan\theta[2+\nu(1+\cos\theta)]}{\delta}, \tag{4.11}$$

with the applied end force $\mathcal{T} = \boldsymbol{\mathcal{F}}\cdot\boldsymbol{D}_3$ and twisting moment $\mathcal{M} = \sin\theta(1+\cos\theta)/\delta$. Finally, equations (3.32) and (3.33) yield

$$\rho(\xi) = \left(\mathcal{T} - \frac{\sin^2\theta}{\delta^2}\right)\frac{\sin\theta\tan\theta}{\delta}, \tag{4.12}$$

with $\rho > 0$ corresponding to an outward-pointing radial reaction pressure. In particular, the free helix is associated with a null reaction pressure corresponding to an axial force $\mathcal{T} = \sin^2\theta/\delta^2$. The post-buckling equilibrium, therefore, satisfies $\mathcal{M}/\sqrt{\mathcal{T}} = 1+\cos\theta$, a well-known result from rod theory (see for instance [47,48]). The influence of the rod axial extensibility on these results is investigated in [44].

(c) Helical conduit

The progressive buckling of an initially straight elastic rod constrained inside a helical conduit is investigated in the following. Although axially unconstrained, i.e. free to flow in/out of the conduit, the rod is assumed to be transversally clamped on the conduit axis at both extremities and subjected to an end torque $\mathcal{M}_3(1) = \mathcal{M}$ and axial force $\mathcal{F}_3(1) = \mathcal{T}$ (figure 3*a*). Assuming the rod to be weightless and maintaining the end torque constant, the magnitude of the axial force is progressively increased until the rod contacts the restraint and a discrete contact subsequently emerges. The constraint considered in the present application is defined by its helical axis, with pitch angle $\Theta = \pi/4$ and radius $\Sigma = R/L = (\pi\sqrt{2})^{-1}$, and constant clearance $\epsilon = Q/L$ where the length $L = \pi R/\sin\Theta$ of the problem under consideration corresponds to half a helical turn. Both clearances $\epsilon = 1/40$ and $1/20$ are investigated. Anticipating the discrete contact to appear at midspan $\xi = 1/2$ for symmetry reasons, the attached $\{\boldsymbol{D}_j\}$-basis is chosen to be the Bishop frame aligned with the Frenet–Serret apparatus at this point.

Although the present application shares multiple features with the problem of an elastica constrained inside a tube that has been investigated in [53–55], it differs by the unprescribed

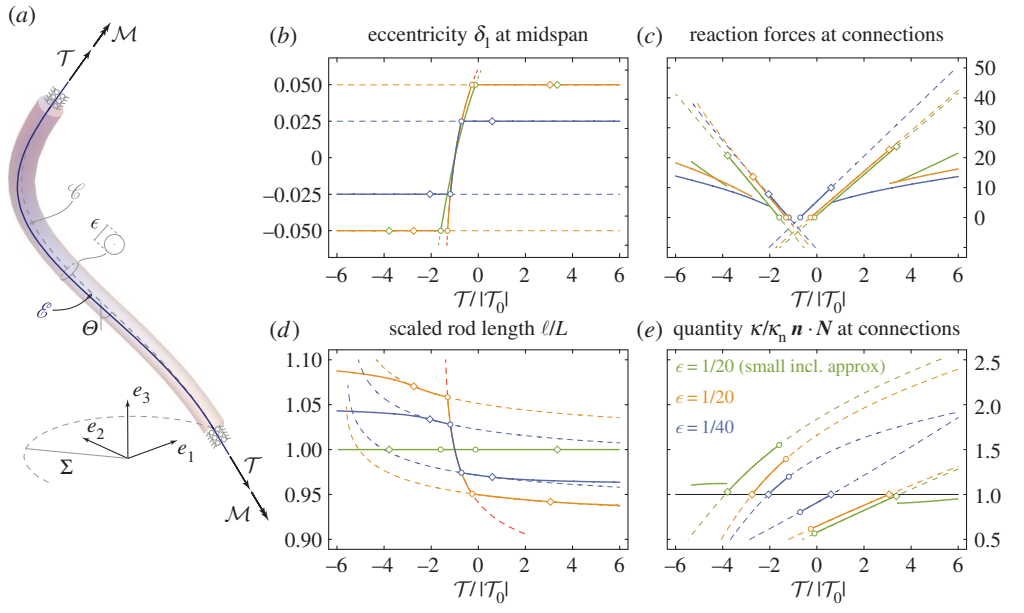

Figure 3. Progressive buckling of an initially straight elastic rod constrained inside a helical conduit and subjected to an end torque $\mathcal{M} = -1$ and axial force $\mathcal{T}$. (*a*) Description of the problem under consideration. (*b*) Eccentricity δ_1 at midspan, (*c*) reaction force $\mathcal{R}$ at the discrete contact, (*d*) scaled unstretched length of the rod ℓ/L and (*e*) rod curvature κ/κ_n at midspan as functions of the end force $\mathcal{T}/|\mathcal{T}_0|$. Results obtained for $\epsilon = 1/40$ and $\epsilon = 1/20$ are plotted in blue and orange, respectively; the small inclination approximation for $\epsilon = 1/20$ is presented in green. Circles mark the appearance of the discrete contacts and squares identify the transition from discrete to continuous contact. (Online version in colour.)

nature of the rod length, i.e. self-feeding. Indeed, while the distance between the extremities of a rod of finite length evolves as a result of the loading, this distance is kept constant in the present analysis and the rod length freely adapts to the loading.

Before analysing the initial contact-free and the subsequent discrete and continuous contact phases of this constrained buckling for $\nu = \frac{1}{3}$, details of the numerical implementation are introduced below.

(i) Numerical implementation

Various numerical methods have been applied to two-point boundary-value problems [56]. The so-called shooting method, which combines a root-finding algorithm and a high-order differential equation solver, has been frequently applied to the Lagrangian problem associated with rods of known length [5,34,55]. Although this numerical technique has also been successfully extended to the Lagrangian free boundary-value problem associated with a planar elastica and its Eulerian reformulation [22], a collocation method was favoured to treat the mixed-order system of nonlinear ordinary differential equations (3.32)–(3.37) and the boundary conditions (3.44)–(3.45) constituting the boundary-value problem under consideration.

Defining a partition Π of the domain $[0,1]$ constituted of N subintervals, an approximate solution $\{\boldsymbol{\delta}^*, \varphi^*, \boldsymbol{\mathcal{F}}^*\}$ is formed as a linear combination of a suitable set of functions, the coefficients of which being determined by requiring the approximate solution to satisfy the boundary conditions as well as the differential equations at certain points [57]. For reasons of efficiency, stability and flexibility in order and continuity, *B*-splines are chosen as basis functions [58] such that

$$\boldsymbol{\delta}^* \in \mathcal{P}_{k+3,\Pi} \cap C^2[0,1], \tag{4.13}$$

$$\varphi^* \in \mathcal{P}_{k+2,\Pi} \cap C^1[0,1] \tag{4.14}$$

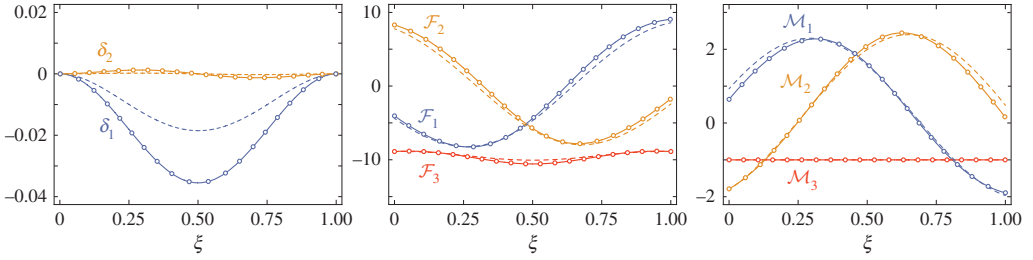

Figure 4. Projections $\delta_i(\xi)$ $(i = 1, 2)$ of the eccentricity vector and components of the internal force $\mathcal{F}_j(\xi)$ and moment $\mathcal{M}_j(\xi)$ $(j = 1, 2, 3)$ as functions of the Eulerian curvilinear coordinate ξ for $\mathcal{M} = -1$ and $\mathcal{T}/|\mathcal{T}_0| = -1.25$. The exact Eulerian formulation (solid line) is compared to both the small inclination approximation (dashed line) and the Lagrangian formulation (line with circles). (Online version in colour.)

and
$$\boldsymbol{\mathcal{F}}^* \in \mathcal{P}_{k+1,\Pi} \cap C^0[0,1], \tag{4.15}$$

where $k \geq 3$ is the number of collocation points per subinterval and $\mathcal{P}_{n,\Pi}$ is the set of all piecewise polynomial functions of order n on the partition Π. The unknown B-spline coefficients are determined by solving the nonlinear system of $6kN$ equations, obtained by collocating the governing equations (3.32)–(3.37) at Gaussian points, and imposing the 11 boundary conditions. This method has been implemented in Matlab by combining the *Spline Toolbox* [59] to evaluate the B-splines and their derivatives with a *line search* (or backtracking) algorithm [60] to solve the nonlinear system of collocation equations.

(ii) Free rod

The initial configuration is chosen to be the helical deformation characterized by a uniformly null eccentricity vector; this state is, however, not to be confused with the straight stress-free configuration $\mathscr{E}^0$ that is only observable in helical conduits with $\epsilon \geq \Sigma$. Following a procedure similar to the one presented in §4b but considering solutions that are not homoclinic to the straight configuration, one may solve the governing equations (3.32)–(3.37) with the boundary conditions $\{\mathcal{F}_3(0) = \mathcal{T}, \mathcal{M}_3(0) = \mathcal{M}\}$. Hence, the axial end force $\mathcal{T} = \mathcal{T}_0$ required to maintain the rod on the constraint axis is obtained by imposing $\rho(\xi) = 0$, that is

$$\Sigma^2 \mathcal{T}_0 = (\Sigma \mathcal{M} - \sin\Theta\cos\Theta)\sin\Theta\cos\Theta. \tag{4.16}$$

For values of the parameters associated with the problem under consideration and $\mathcal{M} = -1$, this relation yields $\mathcal{T}_0 = -7.156$ (questionably achievable with actual materials.)

Maintaining the torque $\mathcal{M}$ constant, the magnitude of the end force $\mathcal{T}$ is progressively increased causing the rod to gradually leave the constraint axis. Results obtained by means of the *exact* Eulerian formulation are compared with both the small inclination approximation (cf. appendix B) and the conventional Lagrangian formulation in figure 4 for $\mathcal{T}/|\mathcal{T}_0| = -1.25$. Although the Eulerian and Lagrangian formulations yield virtually identical results, the small inclination approximation underestimates the magnitude of the rod relative deflection; the overall profile of this solution being, however, coherent. This inaccuracy, due to the large curvature $\mathcal{K} = \pi\sin\Theta$ of the reference curve in spite of the smallness of ϵ, is expected to cause subsequent issues related to the non-penetration condition such as the detection of emerging contacts or the distinction between continuous and discrete contacts. This is further illustrated in the following.

It is also seen that the magnitude of the eccentricity vector is maximal at midspan where $\delta_2 = 0$ such that the emergence of a contact between the rod and the constraint can readily be verified by ensuring that $|\delta_1| < \epsilon$ at $\xi = 1/2$. The evolution of the eccentricity δ_1 at midspan is pictured in figure 3*b* as a function of the end force $\mathcal{T}/|\mathcal{T}_0|$; both the results obtained by means of the exact Eulerian formulation and the small inclination approximation are presented. Additionally, the *self-feeding* ability characterizing the proposed method is emphasized in figure 3*d* as the scaled rod

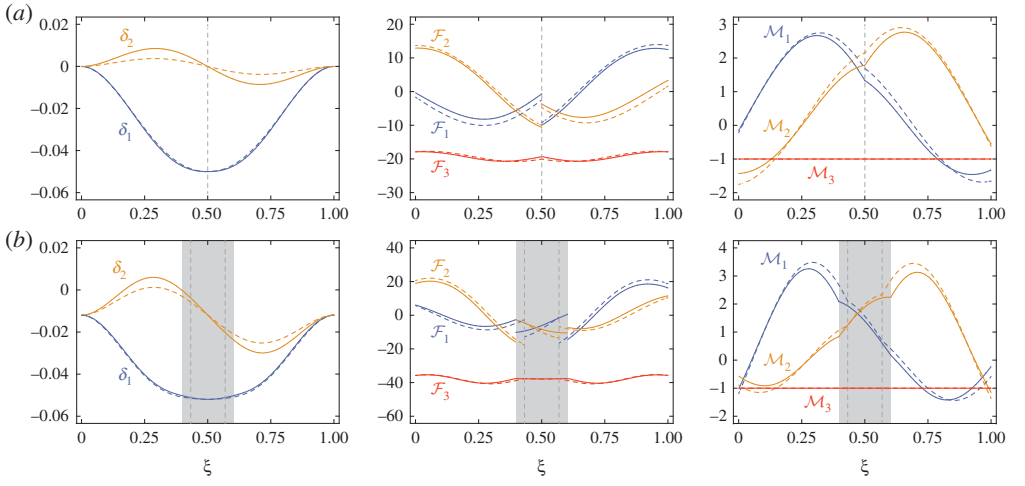

Figure 5. Projections $\delta_i(\xi)$ $(i=1,2)$ of the eccentricity vector and components of the internal force $\mathcal{F}_j(\xi)$ and moment $\mathcal{M}_j(\xi)$ $(j=1,2,3)$ as functions of the Eulerian curvilinear coordinate ξ for $\epsilon=1/20$, $\mathcal{M}=-1$ and (*a*) $\mathcal{T}/|\mathcal{T}_0|=-2.5$, (*b*) $\mathcal{T}/|\mathcal{T}_0|=-5$. The exact Eulerian formulation (solid lines) is compared to the small inclination approximation (dashed lines). Vertical dotted lines mark the positions of discrete contacts while greyed regions delimit the continuous contact. (Online version in colour.)

length ℓ/L, which typically corresponds to the domain of the classical Lagrangian formulation, is seen to freely evolve as a result of the loading.

(iii) Discrete contact

As the eccentricity $\|\boldsymbol{\delta}\|$ reaches the clearance ϵ, a discrete contact emerges between the rod and the constraint giving rise to a reaction force $\boldsymbol{\mathcal{R}}=[\![\boldsymbol{\mathcal{F}}-\mathcal{F}_3\boldsymbol{d}_3]\!]$ aligned with the local normal to the constraint surface and balancing the discontinuity in the shear force. Here, double brackets denotes the increment of the quantity across a discontinuity, e.g. $[\![\boldsymbol{\mathcal{F}}]\!]=\boldsymbol{\mathcal{F}}^+-\boldsymbol{\mathcal{F}}^-$ with the superscripts $+$ and $-$ indicating the two sides of the contact. The magnitude of this reaction force being *a priori* unknown, the global problem is partitioned into two elementary boundary-value problems, each corresponding to a rod segment free of contact. Although both the position and inclination of the rod are prescribed at the extremities of the global problem, only the magnitude of the eccentricity vector is known at the junction of the two elementary problems. Resorting to a shooting method [56], the missing boundary conditions are substituted with educated guesses and the rod integrity is restored by ensuring the continuity of the internal moment across the contact, i.e. $[\![\boldsymbol{\mathcal{M}}]\!]=\boldsymbol{0}$.

The magnitude $\mathcal{R}>0$ of the radial reaction and the scaled rod length ℓ/L are presented in figure 3*c* and *d*, respectively, as the end force varies. For consistency purposes with the preceding phase of the loading, these quantities are plotted in the scaling associated with the global problem. Points marking the appearance of the discrete contact are identified with circles. As anticipated, the small inclination approximation is seen to slightly overestimate the magnitude of the end force at which the contact emerges and, therefore, underestimate the intensity of the reaction force (for the same end force.) Owing to the symmetry of the rod-deformed configuration, the position of the discrete contact along the global problem is, however, properly identified. Fields obtained with the Eulerian formulation and its small inclination approximation are depicted in figure 5*a* for $\epsilon=1/20$ and $\mathcal{T}/|\mathcal{T}_0|=-2.5$. Again, despite the magnitude of the curvature of the reference curve, the two formulations yield reasonably coherent results, both preserving the rod integrity along the global problem. The localized reaction force arising at the discrete contact and the associated jump discontinuity in the shear force may additionally be shown [44] to generate finite jump

discontinuities in the first derivatives of the rod curvature and axial force whose magnitudes are proportional to $\mathcal{R}$.

Further increasing the magnitude of the end force may, however, lead to a violation of the unilateral contact condition and an additional restriction on the curvatures of both the rod and the constraint surface at the contact point should be considered. This criterion, which also marks the transition form discrete to continuous contact, ensures that the normal curvature of the constraint surface is smaller than the curvature of the osculating circle to the space curve $\mathscr{E}$ at the contact point.

(iv) Continuous contact

Along a continuous contact, the rod curvature κ can be decomposed between its normal κ_n and geodesic κ_g components according to [39]

$$\kappa \boldsymbol{n} = \kappa_\mathrm{n} \boldsymbol{N} + \kappa_\mathrm{g} \boldsymbol{N} \times \boldsymbol{d}_3, \tag{4.17}$$

where $\boldsymbol{N}$ is the inward pointing unit normal to the constraint surface. While $\boldsymbol{N} = -\boldsymbol{D}_1$ for the inner ($\delta_1 = \epsilon$) and $\boldsymbol{N} = \boldsymbol{D}_1$ for the outer ($\delta_1 = -\epsilon$) discrete contact, it can be shown that, due to the symmetry of the rod-deformed configuration, the unit normal vector to $\mathscr{E}$ reads $\boldsymbol{n} = \boldsymbol{D}_1$ at these points irrespectively of the contacting side. Additionally, following Euler's theorem, the normal curvature reads

$$\kappa_\mathrm{n} = \mathcal{K}_1 \sin^2\theta + \mathcal{K}_2 \cos^2\theta, \tag{4.18}$$

with the principal curvatures of the constraint surface given by $\mathcal{K}_1 = 1/\epsilon$ and $\mathcal{K}_2 = \mathcal{K}/(\epsilon\mathcal{K} \pm 1)$ for the outer (+) and inner (−) contacts, respectively. Owing to the definition of the constraint, the principal vectors associated with the principal curvatures coincide with $\boldsymbol{D}_2$ and $\boldsymbol{D}_3$ and the angle θ is defined as the inclination of the director $\boldsymbol{d}_3$ on the reference curve according to equation (3.12). Therefore, projecting equation (4.17) on the unit normal vector $\boldsymbol{n} = \pm\boldsymbol{N}$, it can readily be shown that the contacts remain discrete provided the rod curvature satisfies $\kappa/\kappa_\mathrm{n}\boldsymbol{n} \cdot \boldsymbol{N} \geq 1$. Considering expression (4.18) for the normal curvature κ_n and the above-mentioned definitions of the principal curvatures $\mathcal{K}_1$ and $\mathcal{K}_2$, this relation yields

$$\kappa \leq \frac{\epsilon\mathcal{K} - \sin^2\theta}{\epsilon(\epsilon\mathcal{K} - 1)} \quad \text{and} \quad \kappa \geq \frac{\epsilon\mathcal{K} + \sin^2\theta}{\epsilon(\epsilon\mathcal{K} + 1)}, \tag{4.19}$$

at the inner and outer contacts, respectively. The quantity $\kappa/\kappa_\mathrm{n}\boldsymbol{n} \cdot \boldsymbol{N}$ is depicted in figure 3*e* as the end force varies. Points marking the transition from discrete to continuous contact, i.e. at which the inequalities are strictly satisfied, are identified with squares.

At this stage of the loading, the method used to solve the discrete contact problem ceases to be valid and the global problem should be partitioned into three elementary boundary-value problems. As the extent and geometry of the central problem, corresponding to the rod in continuous contact with the constraint surface, are *a priori* unknown a shooting method similar to the one previously introduced can be used. Likewise, the missing boundary conditions at the connections between elementary problems are determined by ascertaining the integrity of the rod along the global problem, that is by ensuring the continuity of the internal moment $[\![\boldsymbol{\mathcal{M}}]\!] = \boldsymbol{0}$ and the radial orientation of the localized $\boldsymbol{\mathcal{R}}_l \times \boldsymbol{N} = \boldsymbol{\mathcal{R}}_r \times \boldsymbol{N} = \boldsymbol{0}$ reactions at these connections. Details about this procedure may be found in [44].

The reaction pressure along the continuous contact is indeed supplemented by two concentrated reaction forces, $\boldsymbol{\mathcal{R}}_l$ and $\boldsymbol{\mathcal{R}}_r$, that balance the discontinuity in the shear force at its extremities. At the transition between discrete and continuous contacts (marked by square in figure 3) the length of the continuous contact is null and, due to the symmetry of the problem under consideration, the magnitude of these forces is half that of the localized reaction force prior to the transition. For the same reason, the magnitudes of these forces increase simultaneously as the end force intensifies and the contact length progressively grows. Within the small inclination approximation, rather than converting to a continuous contact, the discrete contact splits as a local penetration is detected prior to reaching $\kappa/\kappa_\mathrm{n}\boldsymbol{n} \cdot \boldsymbol{N} = 1$ (figure 3*e*). The resulting two reaction

forces similarly partition the global problem into three elementary boundary-value problems, each corresponding to a rod segment free of contact. The discrepancy between the solutions obtained with the Eulerian formulation and its small inclination approximation seems to only slightly affect the rod overall response. As shown in figure 5*b* for $\epsilon = 1/20$ and $\mathcal{T}/\mathcal{T}_0 = 5$, the profiles of the eccentricity vector, internal force and moment indeed remain sensibly similar. Finally, while underestimating the length of the central elementary problem, the small inclination approximation overestimates the magnitude of the reaction forces $\boldsymbol{\mathcal{R}}_\mathrm{l}$ and $\boldsymbol{\mathcal{R}}_\mathrm{r}$ due to the absence of reaction pressure along the central elementary problem.

As the magnitude of the axial end force is further increased, the reaction pressure along the central continuous contact becomes locally outward pointing (i.e. negative). This elementary problem must, therefore, be split to allow these parts of the rod to leave the constraint and preserve the validity of the unilateral contact condition. This forthcoming stage of the loading is, however, not analysed here as it is beyond the scope of the paper.

5. Conclusion and limitations

The Eulerian formulation of elastic rods proposed in this paper was motivated by the wealth of biological, medical and engineering applications concerned by the constrained deformation of elastic rods and the need to efficiently solve this class of problems. This formulation hinges on (i) describing the rod-deformed configuration $\mathscr{E}$ by means of its relative deflection with respect to a reference curve $\mathscr{C}$ and (ii) expressing the kinematical as well as mechanical quantities pertaining to the rod in terms of the curvilinear coordinate associated with the reference curve. Both elementary configurations corresponding to segments of rod either in continuous contact with the constraint or free of contact have been investigated simultaneously as they essentially differ by the nature of the body force acting along the rod.

The restatement of the rod local equilibrium in terms of the Eulerian curvilinear coordinate is particularly appropriate to treat free boundary problems associated with rods forced to go through two distinct fixed points in space. This re-parametrization indeed allows to substitute the unknown domain of the problem, namely the rod length, with the length of the reference curve between the extremities of the problem and, therefore, reduce the resolution to that of a classical boundary-value problem. The isoperimetric constraints that would otherwise ensue from a conventional Lagrangian formulation also vanish. Additionally, the *a posteriori* assessment of the unilateral contact condition ensuring that, depending on the context, the rod remains either in continuous contact or free of contact along an elementary problem has been trivialized through the definition of the eccentricity vector. The detection of emerging contacts throughout contact-free problems hence reduces to the comparison of the eccentricity magnitude with the constraint radius. Alternatively, along continuous contacts, the rod is compelled to lie on the constraining surface by imposing the magnitude of this vector.

The proposed formulation reaches its limits with the single-valuedness of the mapping $S(s)$, from Lagrangian to Eulerian coordinates, and its reciprocal $s(S)$, from Eulerian to Lagrangian coordinates. Geometrically, these knotty situations emerge either as a section along the reference curve is crossed multiple times or if the eccentricity vectors at distinct Eulerian coordinates intersect. The former situation, which usually arises in conjunction with deformed configurations characterized by curling, writhing or other solutions involving self-contact such as folding, can be identified by the orthogonality of the director $\boldsymbol{d}_3$ and the tangent vector to the reference curve $\boldsymbol{D}_3$, i.e. situations where $g_3(\xi)$ vanishes at least once along the domain. Alternatively, the singular configuration associated with the latter situation occurs when the eccentricity vector aligns with the normal vector $\boldsymbol{D}_3'$ to the reference curve and its norm is at least equal to the reference curve curvature $\mathcal{K}$, that is when $\boldsymbol{\delta} \cdot \boldsymbol{D}_3' = \delta_1 \mathcal{U}_2 - \delta_2 \mathcal{U}_1 \geq 1$. Interestingly, these two problematic situations are both avoided by ensuring $g_3(\xi)$ to remain strictly positive throughout the domain. Therefore, situations in which the scalar product $\boldsymbol{d}_3 \cdot \boldsymbol{D}_3$ changes sign cannot be captured by the proposed method.

Although the Eulerian formulation proposed in this paper is restricted to quasi-static solutions of the governing equations, it can readily be extended to incorporate rod dynamics by redefining the Jacobians and the eccentricity vector as time-dependent. Similarly, the assumption of frictionless interactions between the rod and the constraint surface can be relaxed. However, it will require to deal with evolutive problems as solutions become then history dependent. Finally, the definition of the constraint surface may be extended to include constraints with non-circular cross sections, e.g. by describing its local geometry in the $\{\boldsymbol{D}_1, \boldsymbol{D}_2\}$-basis, and account for its deformability, which is essential to biomedical applications.

Authors' contributions. The authors have contributed equally to this work.
Competing interests. We have no competing interests.
Funding. A.H. was supported by the National Fund for Scientific Research of Belgium.
Acknowledgements. We thank the anonymous referees for their thorough reading of our manuscript and their salient comments and suggestions.

Appendix A. Intermediate basis

The $\{\boldsymbol{k}_j\}$-basis is the image of the $\{\boldsymbol{D}_j\}$-basis through the rotation mapping $\boldsymbol{D}_3$ on $\boldsymbol{d}_3$. The axis describing the rotation, therefore, reads $\boldsymbol{\vartheta}(\xi) = g_1\boldsymbol{D}_2 - g_2\boldsymbol{D}_1$ such that, upon application of Rodrigues formula [40], the $\boldsymbol{k}_j$'s are given by

$$\boldsymbol{k}_1(S) = \left(1 - \frac{g_1^2}{1+g_3}\right)\boldsymbol{D}_1 - \frac{g_1 g_2}{1+g_3}\boldsymbol{D}_2 - g_1\boldsymbol{D}_3, \tag{A 1}$$

$$\boldsymbol{k}_2(S) = -\frac{g_1 g_2}{1+g_3}\boldsymbol{D}_1 + \left(1 - \frac{g_2^2}{1+g_3}\right)\boldsymbol{D}_2 - g_2\boldsymbol{D}_3 \tag{A 2}$$

and

$$\boldsymbol{k}_3(S) = g_1\boldsymbol{D}_1 + g_2\boldsymbol{D}_2 + g_3\boldsymbol{D}_3, \tag{A 3}$$

where the g_j's are the components of the unit tangent $\boldsymbol{d}_3$ in the basis attached to the reference curve, see (3.7)–(3.9). The components of the Darboux vector $\boldsymbol{U}(S)$ in this basis read

$$\tilde{U}_1(S) = \left(1 - \frac{g_1^2}{1+g_3}\right)U_1 - \frac{g_1 g_2 U_2}{1+g_3} - g_1 U_3, \tag{A 4}$$

$$\tilde{U}_2(S) = -\frac{g_1 g_2 U_1}{1+g_3} + \left(1 - \frac{g_2^2}{1+g_3}\right)U_2 - g_2 U_3 \tag{A 5}$$

and

$$\tilde{U}_3(S) = g_1 U_1 + g_2 U_2 + g_3 U_3, \tag{A 6}$$

with $U_j(S) = \boldsymbol{U}\cdot\boldsymbol{D}_j$.

Appendix B. Small inclination approximation

The developments presented in §3 lead to the rigorous reformulation of the special Cosserat rod theory within the Eulerian framework associated with the reference curve. Although this reformulation hinges on the description of the rod-deformed configuration by means of its relative deflection about $\mathscr{C}$, no assumptions were made on the magnitude of $\boldsymbol{\delta}(\xi)$. Along interior problems, the rod eccentricity is, however, expected to be at most equal to the constraint radius, while for many typical exterior problems, the rod remains within close range of the reference curve such that the norm $\|\boldsymbol{\delta}\|$ be of the order of the constraint radius. The following rescaling of the eccentricity vector is, therefore, naturally proposed

$$\boldsymbol{\delta}(\xi) = \varepsilon\bar{\boldsymbol{\delta}}, \tag{B 1}$$

with $\bar{\boldsymbol{\delta}}(\xi) = \bar{\delta}_1\boldsymbol{D}_1 + \bar{\delta}_2\boldsymbol{D}_2$ and ε a representative value of $\epsilon(\xi)$ along the elementary problem under consideration such that $\|\bar{\boldsymbol{\delta}}\| = \mathcal{O}(1)$ as $\varepsilon \to 0$. For small values of $\|\boldsymbol{\delta}\|$, i.e. for $\varepsilon \ll 1$, the space curve

$\mathscr{E}$ may be seen as a perturbation of the reference curve and the distinction between Eulerian and stretched coordinates becomes negligible provided the rod relative deflection remains reasonably small compared with the radius of curvature of the reference curve. The conditions under which the nonlinear system (3.32)–(3.37) can be simplified accordingly are investigated next.

For eccentricities of order ε such as previously defined, the inclination of the rod on the reference curve is expected to be comparably small, that is $\theta(\xi) = \mathcal{O}(\varepsilon)$ as $\varepsilon \to 0$, and, consequently, the $\{\boldsymbol{k}_j\}$-basis to be expressed as a perturbation of the $\{\boldsymbol{D}_j\}$-basis attached to the reference curve. Expanding the rotation vector $\boldsymbol{\vartheta}(\xi) = \boldsymbol{D}_3 \times \boldsymbol{k}_3$ in powers of ε and inserting the resulting expression in the definition (3.12) of the intermediate basis leads to

$$\boldsymbol{k}_j(\xi) = \boldsymbol{D}_j + \varepsilon \boldsymbol{k}_j^{(1)} + \varepsilon^2 \boldsymbol{k}_j^{(2)} + \mathcal{O}(\varepsilon^3), \tag{B 2}$$

as $\varepsilon \to 0$, where the first corrections read

$$\boldsymbol{k}_j^{(1)}(\xi) = \boldsymbol{\vartheta}^{(1)} \times \boldsymbol{D}_j \quad \text{and} \quad \boldsymbol{k}_j^{(2)}(\xi) = \frac{1}{2}(\boldsymbol{\vartheta}^{(1)} \times \boldsymbol{k}_j^{(1)}), \tag{B 3}$$

such that the intermediate basis remains orthonormal at each order. The vector $\boldsymbol{\vartheta}(\xi)$ being, by definition, orthogonal to $\boldsymbol{D}_3(\xi)$, it may be expressed as

$$\boldsymbol{\vartheta}(\xi) = \varepsilon \boldsymbol{\vartheta}^{(1)} + \varepsilon^3 \boldsymbol{\vartheta}^{(3)} + \mathcal{O}(\varepsilon^5), \tag{B 4}$$

for $\varepsilon \to 0$, where the corrections read $\boldsymbol{\vartheta}^{(k)}(\xi) = \vartheta_{1,k}\boldsymbol{D}_1 + \vartheta_{2,k}\boldsymbol{D}_2$ with $\vartheta_{1,k}(\xi)$ and $\vartheta_{2,k}(\xi)$ functions of the $\bar{\boldsymbol{\delta}}(\xi)$ and $\boldsymbol{\mathcal{U}}(\xi)$ components.

Comparison of expression (B 2) with the definition of the intermediate basis in terms of the $g_j(\xi)$'s (see equations (A 1)–(A 3)) allows to identify the perturbation expansions for the components of the director $\boldsymbol{d}_3$ in terms of the $\bar{\delta}_i(\xi)$s and $\mathcal{U}_j(\xi)$s. Limiting these developments to twist-free $\{\boldsymbol{D}_j\}$-basis, i.e. Bishop frames, the only non-zero components of the Darboux vector $\boldsymbol{\mathcal{U}}(\xi)$ are of the order of the reference curve curvature $\mathcal{K}(\xi) = \sqrt{\mathcal{U}_1^2 + \mathcal{U}_2^2}$. Therefore, redefining these components as

$$\mathcal{U}_1(\xi) = \mathcal{K}\sin\Phi \quad \text{and} \quad \mathcal{U}_2(\xi) = \mathcal{K}\cos\Phi, \tag{B 5}$$

where $\tan\Phi = \mathcal{U}_1/\mathcal{U}_2$ is the angle between the pair $\{\boldsymbol{D}_1, \boldsymbol{D}_2\}$, and the normal and binormal to $\mathscr{C}$, the components (3.41)–(3.43) become

$$g_1(\xi) = \varepsilon\bar{\delta}_1' + \varepsilon^2\mathcal{K}\bar{\delta}_1'(\bar{\delta}_1\cos\Phi - \bar{\delta}_2\sin\Phi) + \mathcal{O}(\varepsilon^3), \tag{B 6}$$

$$g_2(\xi) = \varepsilon\bar{\delta}_2' + \varepsilon^2\mathcal{K}\bar{\delta}_2'(\bar{\delta}_1\cos\Phi - \bar{\delta}_2\sin\Phi) + \mathcal{O}(\varepsilon^3) \tag{B 7}$$

and

$$g_3(\xi) = 1 - \frac{\varepsilon^2}{2}(\bar{\delta}_1'^2 + \bar{\delta}_2'^2) + \mathcal{O}(\varepsilon^3), \tag{B 8}$$

as $\varepsilon \to 0$.

Considering only the leading order terms, the Jacobian of the mapping from stretched to Eulerian coordinates reduces to

$$\tilde{\mathcal{J}}_1(\xi) = 1 + \varepsilon\mathcal{K}(\bar{\delta}_1\cos\Phi - \bar{\delta}_2\sin\Phi) + \mathcal{O}(\varepsilon^2), \tag{B 9}$$

as $\varepsilon \to 0$, which emphasizes that the drift between these two curvilinear coordinates becomes negligible either for reasonably small curvature of the reference curve or when the eccentricity vector $\boldsymbol{\delta}(\xi)$ is orthogonal to the osculating plane to $\mathscr{C}$, i.e. when the eccentricity of the rod does not *contribute* to its curvature. In many applications, the reference curve is only slightly tortuous and its radius of curvature is large compared with the length L of the problem. Hence, assuming the product $\varepsilon\,\mathcal{K} = \mathcal{O}(\varepsilon^2)$ for $\varepsilon \to 0$, the third terms in equations (B 6) and (B 7) become negligible and the Jacobian reduces to $\mathcal{J}_1(\xi) = 1 + \mathcal{O}(\varepsilon^2)$. Consequently, the components (3.38)–(3.40) of the

fictitious twist vector read

$$\tilde{\omega}_1(\xi) = \mathcal{K}\sin\Phi - \varepsilon\bar{\delta}_2'' + \mathcal{O}(\varepsilon^2), \tag{B 10}$$

$$\tilde{\omega}_2(\xi) = \mathcal{K}\cos\Phi + \varepsilon\bar{\delta}_1'' + \mathcal{O}(\varepsilon^2) \tag{B 11}$$

and

$$\tilde{\omega}_3(\xi) = \mathcal{O}(\varepsilon^2), \tag{B 12}$$

for $\varepsilon \to 0$, leading to a substantial simplification of the governing system of equations (3.32)–(3.37)

$$\tilde{\mathcal{F}}_1' + \tilde{\mathcal{F}}_3(\mathcal{K}\cos\Phi + \varepsilon\bar{\delta}_1'') + \tilde{\sigma}_1 = \mathcal{O}(\varepsilon^2), \tag{B 13}$$

$$\tilde{\mathcal{F}}_2' - \tilde{\mathcal{F}}_3(\mathcal{K}\sin\Phi - \varepsilon\bar{\delta}_2'') + \tilde{\sigma}_2 = \mathcal{O}(\varepsilon^2), \tag{B 14}$$

$$\tilde{\mathcal{F}}_3' + \tilde{\mathcal{F}}_2(\mathcal{K}\sin\Phi - \varepsilon\bar{\delta}_2'') - \tilde{\mathcal{F}}_1(\mathcal{K}\cos\Phi + \varepsilon\bar{\delta}_1'') + \tilde{\sigma}_3 = \mathcal{O}(\varepsilon^2), \tag{B 15}$$

$$\varepsilon\bar{\delta}_1''' + \varepsilon\frac{\varphi'}{1+\nu}\bar{\delta}_2'' + \mathcal{K}\left(\Phi' + \frac{\varphi'}{1+\nu}\right)\sin\Phi - \mathcal{K}'\cos\Phi - \tilde{\mathcal{F}}_1 = \mathcal{O}(\varepsilon^2), \tag{B 16}$$

$$\varepsilon\bar{\delta}_2''' - \varepsilon\frac{\varphi'}{1+\nu}\bar{\delta}_1'' - \mathcal{K}\left(\Phi' + \frac{\varphi'}{1+\nu}\right)\cos\Phi - \mathcal{K}'\sin\Phi + \tilde{\mathcal{F}}_2 = \mathcal{O}(\varepsilon^2) \tag{B 17}$$

and

$$\varphi'' = \mathcal{O}(\varepsilon^2), \tag{B 18}$$

for $\varepsilon \to 0$ and in the absence of body couple.

References

1. Katopodes FV, Barber JR, Shan Y. 2001 Torsional deformation of an endoscope probe. *Proc. R. Soc. Lond. A* **457**, 2491–2506. (doi:10.1098/rspa.2001.0836)
2. Schneider P. 2003 *Endovascular skills: guidewire and catheter skills for endovascular surgery*. Boca Raton, FL: CRC Press.
3. Inglis T. 1988 *Directional drilling*. vol. 2. Berlin, Germany: Springer.
4. Sampaio JHB. 2008 *Drilling engineering*. Perth, Australia: Curtin University of Technology, Department of Petroleum Engineering.
5. da Fonseca AF, de Aguiar MA. 2003 Solving the boundary value problem for finite Kirchhoff rods. *Phys. D* **181**, 53–69. (doi:10.1016/S0167-2789(03)00070-8)
6. Swigon D, Coleman BD, Tobias I. 1998 The elastic rod model for DNA and its application to the tertiary structure of DNA minicircles in mononucleosomes. *Biophys. J.* **74**, 2515–2530. (doi:10.1016/S0006-3495(98)77960-3)
7. Tobias I, Swigon D, Coleman BD. 2000 Elastic stability of DNA configurations. I. General theory. *Phys. Rev. E* **61**, 747–758. (doi:10.1103/PhysRevE.61.747)
8. Yang Y, Couchman LS. 1997 Elastic theory of nucleosomal DNA. *Proc. R. Soc. Lond. A* **453**, 225–254. (doi:10.1098/rspa.1997.0014)
9. Tu X, Manohar S, Jagota A, Zheng M. 2009 DNA sequence motifs for structure-specific recognition and separation of carbon nanotubes. *Nature* **460**, 250–253. (doi:10.1038/nature08116)
10. Goriely A, Neukirch S. 2006 Mechanics of climbing and attachment in twining plants. *Phys. Rev. Lett.* **97**, 184302. (doi:10.1103/PhysRevLett.97.184302)
11. Goriely A, Robertson-Tessi M, Tabor M, Vandiver R. 2008 Elastic growth models. In *Mathematical modelling of biosystems*. Applied Optimization 102, pp. 1–44. Berlin, Germany: Springer.
12. Chen J-S, Li C-W. 2007 Planar elastica inside a curved tube with clearance. *Int. J. Solids Struct.* **44**, 6173–6186. (doi:10.1016/j.ijsolstr.2007.02.021)
13. Denoël V. 2008 Advantages of a semi-analytical approach for the analysis of an evolving structure with contacts. *Commun. Numer. Methods Eng.* **24**, 1667–1683. (doi:10.1002/cnm.1059)
14. Friedman A. 2000 Free boundary problems in science and technology. *Not. AMS* **47**, 854–861.
15. Donea J, Huerta A, Ponthot J-P, Rodríguez-Ferran A. 2004 *Arbitrary Lagrangian–Eulerian methods*, ch. 14, pp. 413–437. New York, NY: John Wiley & Sons, Ltd.
16. Guarracino F, Mallardo V. 1999 A refined analytical analysis of submerged pipelines in seabed laying. *Appl. Ocean Res.* **21**, 281–293. (doi:10.1016/S0141-1187(99)00020-6)

17. Stump D, van der Heijden G. 1999 Matched asymptotic expansions for bent and twisted rods: applications for cable and pipeline laying. *J. Eng. Math.* **38**, 13–31. (doi:10.1023/A:1004634100466)
18. Bosi F, Misseroni D, Dal Corso F, Bigoni D. 2014 An elastica arm scale. *Proc. R. Soc. A* **470**, 20140232. (doi:10.1098/rspa.2014.0232)
19. Bosi F, Misseroni D, Dal Corso F, Bigoni D. 2015 Self-encapsulation, or the 'dripping' of an elastic rod. *Proc. R. Soc. A* **471**, 20150195. (doi:10.1098/rspa.2015.0195)
20. Chen J-S, Ro W-C. 2010 Deformations and stability of an elastica subjected to an off-axis point constraint. *J. Appl. Mech.* **77**, 20140232 031006. (doi:10.1115/1.4000426)
21. Denoël V, Detournay E. 2009 The problem of a drillstring inside a curved borehole: a perturbed eulerian approach. In *First Int. Colloquium on Non-linear Dynamics of Deep Drilling Systems*, March 2009, pp. 89–95. Liège, Belgium: University of Liège.
22. Denoël V, Detournay E. 2011 Eulerian formulation of constrained elastica. *Int. J. Solids Struct.* **48**, 625–636. (doi:10.1016/j.ijsolstr.2010.10.027)
23. Bastl B, Jüttler B, Lávička M, Schulz T, Šír Z. 2014 On the parameterization of rational ringed surfaces and rational canal surfaces. *Math. Comput. Sci.* **8**, 299–319. (doi:10.1007/s11786-014-0192-y)
24. Dill E. 1992 Kirchhoff's theory of rods. *Arch. Hist. Exact Sci.* **44**, 1–23. (doi:10.1007/BF00379680)
25. Antman S. 2005 *Nonlinear problems of elasticity*, ch. 8, vol. 107, 3rd edn. Berlin, Germany: Springer.
26. Goss VGA. 2003 Snap buckling, writhing and loop formation in twisted rods. PhD thesis, University of London, Center for Nonlinear Dynamics, London, UK.
27. Goyal S, Perkins N. 2008 Looping mechanics of rods and DNA with non-homogeneous and discontinuous stiffness. *Int. J. Non-Linear Mech.* **43**, 1121–1129. (doi:10.1016/j.ijnonlinmec.2008.06.013)
28. Goyal S, Perkins N, Lee C. 2005 Nonlinear dynamics and loop formation in kirchhoff rods with implications to the mechanics of DNA and cables. *J. Comput. Phys.* **209**, 371–389. (doi:10.1016/j.jcp.2005.03.027)
29. Antman S, Kenney C. 1981 Large buckled states of nonlinearly elastic rods under torsion, thrust, and gravity. *Arch. Ration. Mech. Anal.* **76**, 289–338. (doi:10.1007/BF00249969)
30. Kehrbaum S, Maddocks J. 1997 Elastic rods, rigid bodies, quaternions and the last quadrature. *Phil. Trans. R. Soc. Lond. A* **355**, 2117–2136. (doi:10.1098/rsta.1997.0113)
31. Shi Y, Hearst J. 1994 The Kirchhoff elastic rod, the nonlinear Schrödinger equation, and DNA supercoiling. *J. Chem. Phys.* **101**, 5186. (doi:10.1063/1.468506)
32. Tan Z, Witz J. 1995 *On the deflected configuration of a slender elastic rod subject to parallel terminal forces and moments*. *Proc. R. Soc. Lond. A* **449**, 337–349. (doi:10.1098/rspa.1995.0048)
33. Bergou M, Wardetzky M, Robinson S, Audoly B, Grinspun E. 2008 Discrete elastic rods. *ACM Trans. Graph.* **27**, 63:1–63:12.
34. van der Heijden G, Neukirch S, Goss V, Thompson J. 2003 Instability and self-contact phenomena in the writhing of clamped rods. *Int. J. Mech. Sci.* **45**, 161–196. (doi:10.1016/S0020-7403(02)00183-2)
35. Crank J, Gupta RS. 1972 A moving boundary problem arising from the diffusion of oxygen in absorbing tissue. *IMA J. Appl. Math.* **10**, 19–33. (doi:10.1093/imamat/10.1.19)
36. AliAbadi M, Ortiz E. 1998 Numerical treatment of moving and free boundary value problems with the tau method. *Comput. Math. Appl.* **35**, 53–61. (doi:10.1016/S0898-1221(98)00044-3)
37. Cartan E. 1937 *La théorie des groupes finis et continus et la géométrie différentielle: traitées par la méthode du repère mobile*. Paris, France: Gauthier-Villars.
38. Bishop RL. 1975 There is more than one way to frame a curve. *Am. Math. Mon.* **82**, 246–251. (doi:10.2307/2319846)
39. Pressley A. 2010 *Elementary differential geometry*. London, UK: Springer.
40. Cheng H, Gupta KC. 1989 An historical note on finite rotations. *J. Appl. Mech.* **56**, 139–145. (doi:10.1115/1.3176034)
41. Bergou M, Audoly B, Vouga E, Wardetzky M, Grinspun E. 2010 Discrete viscous threads. *ACM Trans. Graph.* **29**, 116:1–116:10.
42. Huynen A, Detournay E, Denoël V. 2015 Surface constrained elastic rods with application to the sphere. *J. Elast.* **123**, 203–223. (doi:10.1007/s10659-015-9555-0)
43. Langer J, Singer DA. 1996 Lagrangian aspects of the Kirchhoff elastic rod. *SIAM Rev.* **38**, 605–618. (doi:10.1137/S0036144593253290)

44. Huynen A. 2015 Eulerian formulation of spatially constrained elastic rods. PhD thesis, University of Minneapolis and University of Liège.
45. Goriely A, Tabor M. 1997 Nonlinear dynamics of filaments: III. instabilities of helical rods. *Proc. R. Soc. Lond. A* **453**, 2583–2601. (doi:10.1098/rspa.1997.0138)
46. Seemann W. 1996 Deformation of an elastic helix in contact with a rigid cylinder. *Arch. Appl. Mech.* **67**, 117–139. (doi:10.1007/BF00787145)
47. Thompson J, Champneys A. 1996 From helix to localized writhing in the torsional post-buckling of elastic rods. *Proc. R. Soc. Lond. A* **452**, 117–138. (doi:10.1098/rspa.1996.0007)
48. Thompson J, Silveira M, van der Heijden G, Wiercigroch M. 2012 Helical post-buckling of a rod in a cylinder: with applications to drill-strings. *Proc. R. Soc. A* **468**, 1591–1614. (doi:10.1098/rspa.2011.0558)
49. van der Heijden G. 2001 The static deformation of a twisted elastic rod constrained to lie on a cylinder. *Proc. R. Soc. Lond. A* **457**, 695–715. (doi:10.1098/rspa.2000.0688)
50. van der Heijden GHM, Champneys A, Thompson J. 2002 Spatially complex localisation in twisted elastic rods constrained to a cylinder. *Int. J. Solids Struct.* **39**, 1863–1883. (doi:10.1016/S0020-7683(01)00234-7)
51. Love A. 1927 *A treatise on the mathematical theory of elasticity*. 4th edn. Cambridge, UK: Cambridge University Press.
52. van der Heijden G, Thompson J. 2000 Helical and localised buckling in twisted rods: a unified analysis of the symmetric case. *Nonlin. Dyn.* **21**, 71–99. (doi:10.1023/A:1008310425967)
53. Chen J-S, Li H-C. 2011 On an elastic rod inside a slender tube under end twisting moment. *J. Appl. Mech.* **78**, 041009. (doi:10.1115/1.4003708)
54. Fang J, Li S-Y, Chen J-S. 2013 On a compressed spatial elastica constrained inside a tube. *Acta Mech.* **224**, 2635–2647. (doi:10.1007/s00707-013-0889-z)
55. Li S-Y, Chen J-S. 2014 A twisted elastica constrained inside a tube. *Eur. J. Mech. A* **44**, 61–74. (doi:10.1016/j.euromechsol.2013.10.006)
56. Ascher U, Mattheij R, Russell RD. 1995 *Numerical solution of boundary value problems for ordinary differential equations*. Philadelphia, PA: Society for Industrial and Applied Mathematics.
57. de Boor C, Swartz B. 1973 Collocation at gaussian points. *SIAM J. Numer. Anal.* **10**, 582–606. (doi:10.1137/0710052)
58. Ascher U, Christiansen J, Russell RD. 1979 A collocation solver for mixed order systems of boundary value problems. *Math. Comput.* **33**, 659–679. (doi:10.1090/S0025-5718-1979-0521281-7)
59. de Boor C. 2005 Spline toolbox for use with MATLAB: user's guide. Natick, MA: MathWorks.
60. Dennis JE, Schnabel RB. 1996 *Numerical methods for unconstrained optimization and nonlinear equations*. Philadelphia, PA: Society for Industrial and Applied Mathematics.